

Mechanistic Insights into the Structural Stability of Collagen-Containing Biomaterials Such as Bones and Cartilage

Nidhi Tiwari, Sungsool Wi, Frederic Mentink-Vigier, and Neeraj Sinha*

Cite This: *J. Phys. Chem. B* 2021, 125, 4757–4766

Read Online

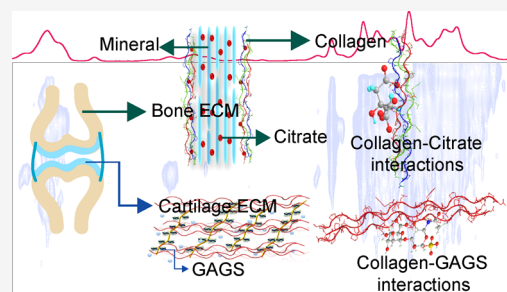
ACCESS |

Metrics & More

Article Recommendations

Supporting Information

ABSTRACT: Structural stability of various collagen-containing biomaterials such as bones and cartilage is still a mystery. Despite the spectroscopic development of several decades, the detailed mechanism of collagen interaction with citrate in bones and glycosaminoglycans (GAGs) in the cartilage extracellular matrix (ECM) in its native state is unobservable. We present a significant advancement to probe the collagen interactions with citrate and GAGs in the ECM of native bones and cartilage along with specific/non-specific interactions inside the collagen assembly at the nanoscopic level through natural-abundance dynamic nuclear polarization-based solid-state nuclear magnetic resonance spectroscopy. The detected molecular-level interactions between citrate–collagen and GAG–collagen inside the native bone and cartilage matrices and other backbone and side-chain interactions in the collagen assembly are responsible for the structural stability and other biomechanical properties of these important classes of biomaterials.



1. INTRODUCTION

Higher vertebrates' skeleton is made up of a highly specialized form of connective tissue consisting of bones and cartilage.¹ These connective tissues are primarily composed of a fibrous extracellular matrix (ECM), involved in diverse physiological roles, including nutrient storage, endocrine function, and providing structural integrity.² Collagen is the most abundant structural component in the ECM of these connective tissues, which forms a scaffold to provide strength and structure, known for its wide range of functions, including local storage, entrapment, delivery of growth factors, tissue morphogenesis, and tissue repair.^{3,4} The most common natural occurrence in all connective tissues and a broad range of functional behaviors make it a widely studied biological system. Most of the studies had been done using extracted collagen, model peptides, and molecular dynamics simulation.^{5–7} The absolute native environment of collagen in connective tissues is formed with other ECM components and interactions among them and hence responsible for different structural arrangements than the extracted form of collagen.⁸ The collagen protein possesses a triple helical structure, which is a polypeptide chain primarily consisting of a unique amino acid (AA) sequence of glycine (Gly), proline (Pro), and hydroxyproline (Hyp) as repeating units.⁹ The triple-helical fibrillar structure of collagen is stabilized by water-mediated hydrogen bonds and a stereo-electric effect of the Hyp ring, which endorses the non-specific self-association, along with charged and hydrophobic interactions, which confer specificity and a high affinity for self-association.^{10–15} The structural and functional role, along with unique biomechanical properties of these connective tissues, including load-bearing capacity, tensile and shear strength, and

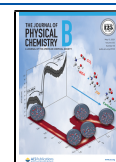
shock absorption, is directly governed by collective intra- and intermolecular interactions between its ECM components. Mapping these interactions at the atomic level in native bones and cartilage can provide better insights into their working mechanism.¹⁶

Bone mineralization is a crucial step in bone formation. Collagen present in bones provides a template for the deposition of calcium phosphate (CaP) and promotes the self-assembly of small amorphous CaP, and other bone ECM components such as water and lipid are essential to manifest the process.^{17–20} Citrate is an abundant structural component of the bone ECM, constituting 1–5% weight of the bone organic matrix,²¹ has a high binding affinity to calcium stored in the hard tissue, and plays a pivotal role in regulating metabolic functions and maintaining the structural integrity of the bone.²² Citrate plays a significant role in improving the mineralization of collagen by facilitating the intrafibrillar formation of hydroxyapatite (HAP).^{23,24} Besides, citrate has been widely used as a medical drug in osteoporosis, and vitamin-D-deficient rickets disease is treated with vitamin-D and citrate therapy.²⁵ Recent NMR/X-ray studies of bones have identified that citrate is a bound component of the apatite nanocrystal/collagen complex and acts as a bridging element

Received: February 16, 2021

Revised: April 20, 2021

Published: April 30, 2021



between the layers of mineral platelets of the bone.^{24,26,27} Reynolds et al. performed a study that revealed the existence of two distinct pools of citrate in the bone ECM. One pool (~65–80% of the total citrate) is associated with the HAP component, while another pool (~20–35% of the total citrate) is tightly bound to the collagen component of the apatite nanocomposite–collagen complex, detected by wet chemical analysis.²⁸ Citrate bound with HAP is a well-studied phenomenon, while the interaction of citrate with collagen at the molecular/atomic level in the native bone ECM has not been well defined.

In the cartilage ECM, high water content combined with a fibrillar portion (collagen and proteoglycan) provides the load-bearing capacity to the cartilage and enables the low frictional movement to the joints.²⁹ The ECM of cartilage is made up of type II collagen protein (~12 wt %), proteoglycan (~6 wt %), and water (~82 wt %). The polysaccharide chains of proteoglycans consist of chondroitin sulfate (CS), a major component, keratan sulfate, and hyaluronan.^{30–32} Proteoglycan glycosaminoglycan (GAG)–collagen interactions not only contribute to cartilage biomechanics but are also essential to governing the chondrocyte activities and ECM assembly.^{33–36} Few studies in the literature that identify the direct, non-specific interactions between proteoglycan GAGs and the fibrillar collagen network in the cartilage ECM have been reported. Therefore, studying the interaction between two primary constituents of the cartilage ECM is essential to understand the cartilage tissue function and associated diseases.

Due to the complex heterogeneous structure of cartilage and bone ECMs, it is quite challenging for most of the biophysical techniques to investigate such biological systems at the atomic level in their native state. Solid-state nuclear magnetic resonance (ssNMR) is a well-established and non-destructive technique capable of studying the complex heterogeneous morphology of bone and cartilage ECMs in their native state.^{37,38} Despite advancements in ssNMR instrumentation and methodologies, the low sensitivity must often be compensated by isotopic enrichment. This severely limits the applicability of all these ssNMR methods for atomic-level investigation of different components of bone and cartilage ECMs, where natural isotopic abundance is the main viable approach. Recent advancements in ssNMR instrumentation and methodology had solved the problem of sensitivity enhancement to some extent. ¹H-detected NMR measurements under ultrafast magic-angle spinning (MAS) (>60 kHz) conditions^{39,40} led to an improvement in the spectral resolution of ¹H-detected lineshapes and sensitivity enhancement in bone spectra by suppressing the ¹H–¹H homonuclear dipolar couplings and other ¹H anisotropic interactions, responsible for line broadening in the ¹H NMR spectra. In addition, the recently developed BioSolids CryoProbe facilitated us to get a 3–4-fold sensitivity enhancement in bone spectra^{41,42} at the natural isotopic abundance. The sensitivity gain with both the techniques is not enough for detecting the interaction among the various constituents in bone and cartilage ECMs in their native state. In this context, MAS-dynamic nuclear polarization (MAS-DNP)^{43–47} is an excellent technique to alleviate the inherently low sensitivity of MAS-ssNMR toward the non-isotopically labeled ECMs of bones and cartilage in their native state.

In the present study, we have employed MAS-DNP-enhanced ssNMR methods to the native bone and cartilage

samples to probe the nanoscopic length structure along with associated interactions of both ECMs by utilizing DNP-based two-dimensional (2D) ¹H–¹³C/¹⁵N heteronuclear correlation (HETCOR) and ¹³C–¹³C double quantum (DQ)–single quantum (SQ) NMR experiments in natural abundance.^{48–51} With the help of these experiments, we were able to probe the collagen–citrate (the bone ECM) and collagen–GAG (the cartilage ECM) molecular interactions along with other non-specific and specific interactions present in the collagen assembly at the natural isotopic abundance. These interactions are responsible for the structural stability of these important classes of biomaterials.

2. EXPERIMENTAL SECTION

2.1. MAS-DNP Sample Preparation. All the DNP-ssNMR experiments were performed on the cortical femora bone and articular cartilage of a goat (*Capra hircus*, 2–3 years old). After cleaning, small pieces of full-thickness cartilages were carefully removed from the bones by a scalpel, and small-sized flakes of the bone were obtained by filing the intact bone with the help of a scalpel. About 60 mg of each sample (powdered bone and cartilage tissue sample) was mixed with 60 μ L of nitroxide biradical AMUPOL⁵² 10 mM in 90% D₂O and 10% H₂O in an Eppendorf tube for thorough mixing. The sample mixture was packed into a 3.2 mm thin-walled zirconia rotor with a vessel cap for low-temperature experiments.

2.2. MAS-DNP-ssNMR Parameters. MAS-DNP ssNMR spectra were obtained on a wide-bore 600 MHz Bruker AVANCE III spectrometer equipped with a 395 GHz gyrotron microwave source by employing a 3.2 mm MAS ¹H–¹³C–¹⁵N triple-resonance Bruker probe.⁵³ The sample temperature for DNP experiments under MAS conditions was maintained at about 100 K by flowing a nitrogen gas stream to the sample compartment as well as to the bearing and drive inlets of the MAS controller unit for MAS spinning at $\nu_r = 8$ kHz. The nitrogen gas stream used for both the variable temperature control and the MAS spinning regulation was obtained by evaporation from a liquid nitrogen tower and was fed into the system through the DNP cabinet with an appropriate set of regulations. A saturation recovery pulse sequence was placed along the proton channel before each NMR pulse sequence with an optimal buildup time of about 10 s, while the microwave is continuously irradiated at the sample with an appropriate power. The DNP enhancement factors observed in our ¹H–¹³C and ¹H–¹⁵N CPMAS experiments were about $\epsilon = 30$ and $\epsilon = 30$, respectively. The ¹H and ¹³C 90° pulses used were 2.5 and 3.5 μ s, respectively, for all experiments. The ¹H–¹³C and ¹H–¹⁵N CPMAS pulse parameters employed were $\nu_{1H} = 60 \pm 5$ kHz and $\nu_{13C} = 50 \pm 5$ kHz for 1 ms and $\nu_{1H} = 35 \pm 5$ kHz and $\nu_{15N} = 25 \pm 5$ kHz for 1.5 ms, respectively, by employing ramped (90–110%) spin-lock pulses along the ¹H channel while simultaneously applying a rectangular spin-lock pulse either on ¹³C or ¹⁵N. The basic pulse unit of the PMLG consists of $\{(P)_5(P)_5\}_n$. The ¹H pulse power used during the PMLG mixing was 100 kHz. Thus, the width of the basic pulse unit *P* is 1.41 μ s with $n = 1$. For acquiring a 2D ¹H–*X* (*X* = ¹³C or ¹⁵N) HETCOR spectrum, the dwell time of the indirect time domain was set to $\{(P)_5(P)_5\}_2$ with $n = 2$, which is 28.2 μ s. The pulse power of the SPC-5 sequence block for the ¹³C–¹³C 2D INAD-EQUATE⁵⁴ experiment was $\nu_{13C} = 5\nu_r = 40$ kHz and $\nu_{1H} = 110$ kHz. Typically, 512 and 4096 scans were acquired for obtaining noise-free one-dimensional (1D) ¹H–¹³C and

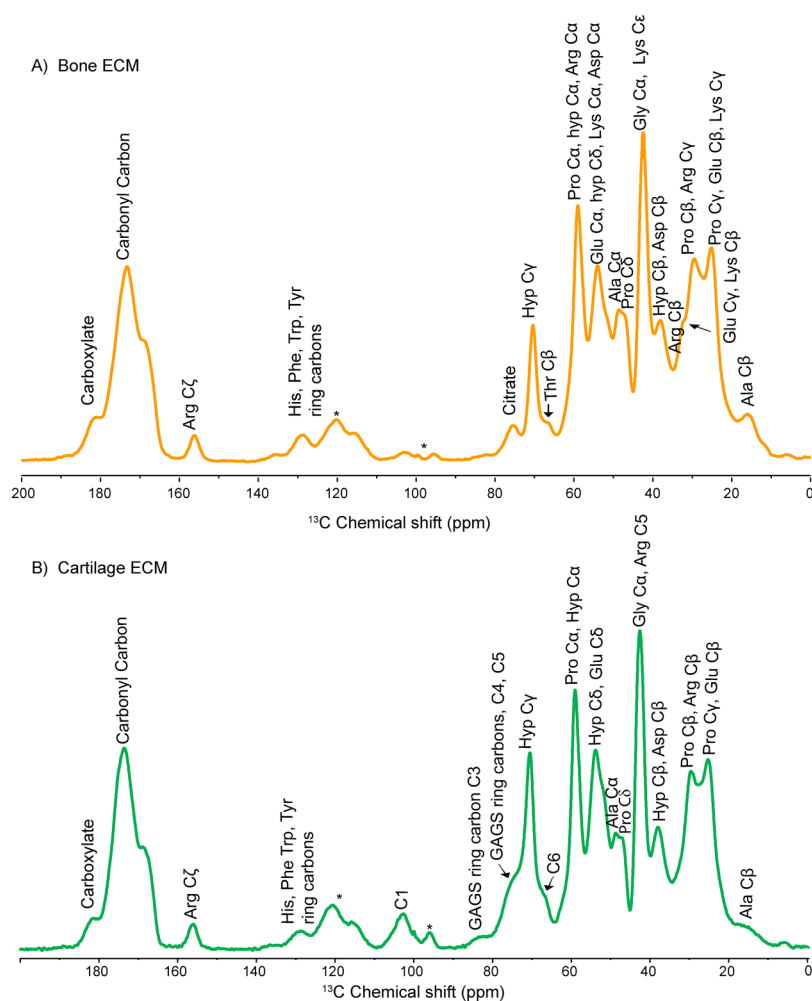


Figure 1. Assigned resonances in natural-abundance DNP-enhanced 1D ^1H - ^{13}C CPMAS spectra of (A) the bone ECM and (B) the cartilage ECM.

^1H - ^{15}N CPMAS spectra, respectively. For obtaining 2D ^1H - ^{13}C HETCOR⁵⁵ and ^{13}C - ^{13}C INADEQUATE experiments, 256 t_1 slices were acquired with 64 scans for each t_1 slice. For conducting a 2D ^1H - ^{15}N HETCOR experiment, 256 t_1 slices were acquired with 256 scans for each t_1 slice. A SPINAL-64⁵⁶ proton decoupling sequence was used during the direct acquisition period, with a 100 kHz decoupling power. Gaussian window function was used for processing the 1D ^1H - ^{13}C and ^1H - ^{15}N CPMAS, 2D ^1H - $^{13}\text{C}/^{15}\text{N}$ HETCOR, and ^{13}C - ^{13}C INADEQUATE spectra.

3. RESULTS AND DISCUSSION

3.1. Enhanced Resonances from Citrate, GAG, and Aromatic AA Residues inside the Bone and Cartilage Matrices. Collagen is an integral part of both bone and cartilage ECMs. The DNP-enhanced 1D ^1H - ^{13}C CPMAS spectrum of collagen protein in the native bone shows ~30-fold sensitivity enhancement in ^{13}C resonances when the microwave is ON (Figure S1A) over that when the microwave is OFF (Figure S1B). We have assigned most of the ^{13}C resonances from the organic matrix in native bone and cartilage ECMs (Figure 1A,B) as per the reported literature.^{8,38,37} Observed ^{13}C resonances from the backbone of collagen protein, including Gly, Pro, and Hyp, are similar to the spectrum recorded with conventional ssNMR methods,

suggesting that the structural integrity of the organic matrix remains unaffected even at low temperatures and after doping with the biradical. Aliphatic residues predominantly dominate the 1D ^1H - ^{13}C CPMAS spectra of collagen. However, a significant signal enhancement is observed in ^{13}C resonances from citrate (74–76 ppm), aromatic AA residues (Phe, Tyr, and His at 129 ppm), and Arg C ζ (156.8 ppm) of collagen protein, which have extremely low abundances in the bone ECM. Similarly, in the cartilage matrix, signal enhancement is observed in ^{13}C resonances from GAG ring carbons (103.6, 84, 76, and 79 ppm), aromatic residues (129 ppm), and Arg C ζ (156.8 ppm).⁵⁸ The complex heterogeneous structure of the cartilage ECM consists of highly mobile GAGs and relatively rigid collagen protein, and a line broadening in a few of ^{13}C resonances is observed. A dominating factor that governs the linewidths of DNP spectra is the formation of a glassy state of the sample under the frozen condition (~100 K) due to the mixing with the DNP juice. The resulted glassy state of sample would increase the heterogeneity of sample that causes the asymmetric broadened line shape, called Czjzek lineshape. (Figure S8), as shown in the 2D ^1H - ^{13}C DNP HETCOR spectrum of the cartilage sample. The major peak around 7 ppm in the projected ^1H spectrum shown on the left in red color is taken as a projection from 57 to 60 ppm along ^{13}C and exhibits the characteristic Czjzek lineshape,^{59,60} an asymmetric

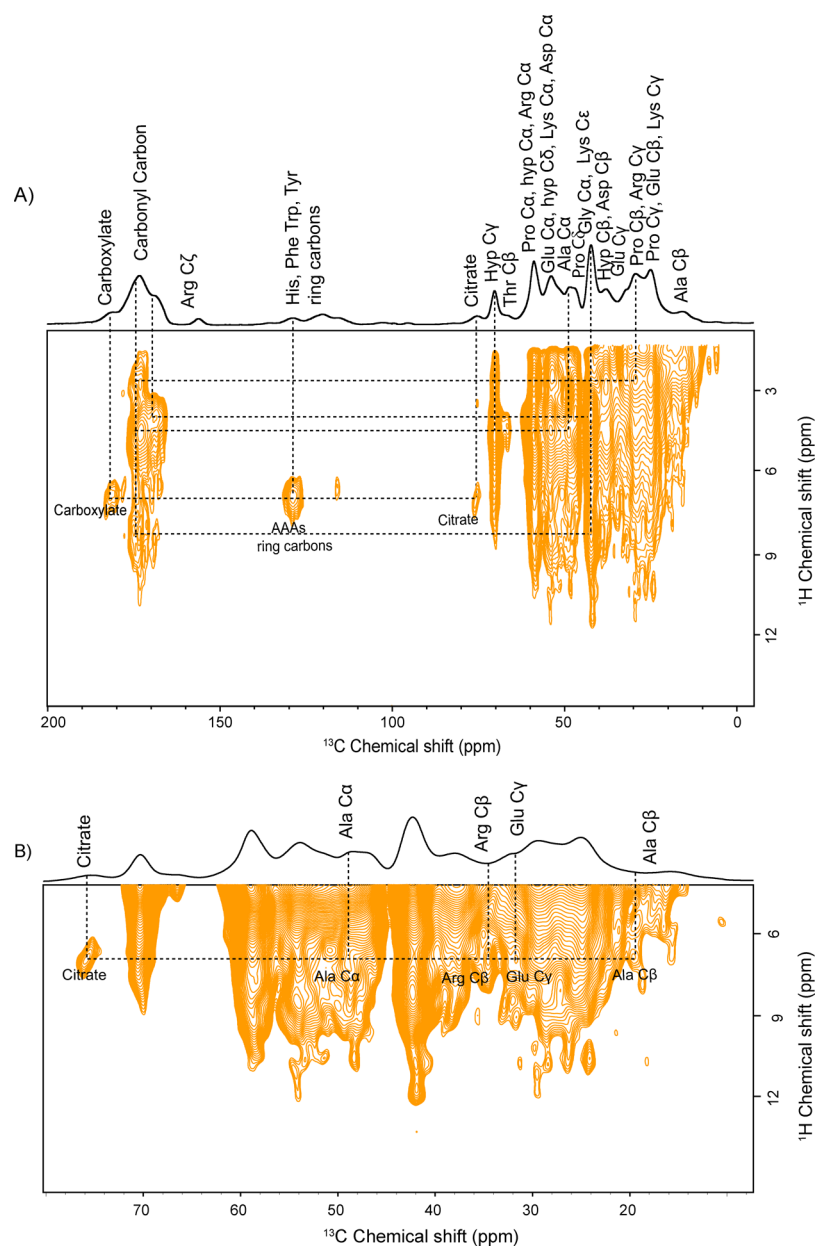


Figure 2. (A) Natural-abundance 2D PMLG ^1H - ^{13}C HETCOR spectrum of the bone ECM and (B) the expanded region of A, showing molecular interaction between citrate and collagen residues along with other molecular interactions represented by the dotted line.

lineshape that results due to the formation of a disordered glassy sample state. In this DNP sample condition, the linewidths coming from the sample's intrinsic heterogeneity in the conformation would be much less than that from the formation of a glassy state after freezing the sample that is mixed with the DNP juice. Under our DNP sampling condition, the paramagnetic contribution to the linewidths of the peaks is negligible.

Overall, an increase in the signal intensity of ^{13}C resonances from the molecules which are present in extremely low concentrations in the matrix of both the cartilage and bone facilitates us to record more advanced DNP-based ssNMR experiments.

3.2. High-Resolution Structural Insights into the Native Bone and Cartilage ECMs. Native collagen and extracted collagen have been extensively studied using ssNMR,^{5,37,57} but its interactions with less abundant

components such as citrate and GAGs in native bone and cartilage ECMs could not have been depicted due to the limited applicability of ssNMR in natural abundance. Therefore, to probe the molecular interactions between collagen and other ECM components of the native bone and cartilage, we performed MAS-DNP-based 2D PMLG ^1H - ^{13}C HETCOR experiments in natural abundance at a cross-polarization (CP) contact time of 200 μs . At 100 μs contact time, 2D PMLG ^1H - ^{13}C HETCOR spectra gave identical results but with a poor signal-to-noise ratio. Intermolecular correlations were observed among various constituents, which are ^1H - ^{13}C dipolar-coupled in their spatial proximity. In the bone ECM, we majorly focused on probing the molecular interactions between citrate and collagen.

Citrate, having three carboxylate groups, is synthesized and produced by osteoblasts during bone formation.²⁸ The major citrate pool is strongly associated with HAP, while ~20–35%

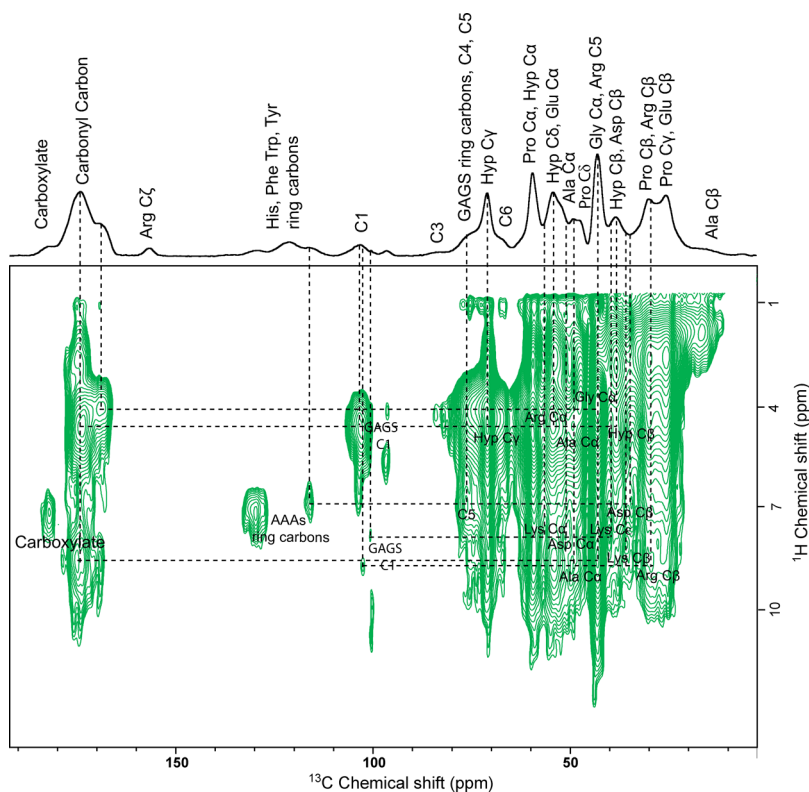


Figure 3. Natural-abundance 2D PMLG ^1H – ^{13}C HETCOR spectrum of the cartilage ECM shows molecular interaction between GAGs and collagen residues along with other molecular interactions represented by the dotted line.

citrate is tightly bound to collagen. The molecular association of citrate with collagen protein at the atomic level is observed in the 2D ^1H – ^{13}C HETCOR spectrum of the bone sample in natural isotopic abundance. Various molecular interactions in the native bone ECM are shown in Figure 2. The chemical structure of the citrate molecule is shown in Figure S3. The citrate chemical shift at 75.8 ppm corresponds to the quaternary carbon of citrate, and protons associated with citrate appear at 2.7–3.5 ppm. Hence, the correlation of quaternary carbon of citrate with collagen residues is due to ^1H – ^{13}C dipolar coupling networks, which are in spatial proximity. The ^1H and ^{13}C slices of the cross-peak of interest from the 2D ^1H – ^{13}C HETCOR spectrum of the bone are given in Figure S4. Molecular interaction between citrate (75.8 ppm) and protons of aromatic AA ring carbons (Phe, Tyr, Trp, and His at 129 ppm) is observed (Figure 2A), showing that citrate is involved in hydrophobic interaction with aromatic AAs of collagen protein. Besides this, citrate shows molecular interaction with the charged residue of collagen protein, including protons of Arg C β (34.6 ppm) and Glu C γ (31.6 ppm), as shown in Figure 2B, suggesting the existence of charge-pair interactions and hydrogen bonding between them. The correlation of protons of Ala C α (48.2 ppm) and Ala C β (19.6 ppm) from collagen protein with citrate shows a non-covalent association with citrate molecules. These findings suggest that collagen protein in the bone ECM may be involved in the citrate homeostasis in the bone metabolic pathway. Besides the collagen–citrate interactions, long-range interactions are seen between aromatic AA ring carbons and the carboxylate group of acidic AA residues such as Glu/Asp. A hydrogen bonding network, as well as some hydrophobic interactions, was observed in the collagen matrix (Figure 2).

The structural–functional mechanism of the cartilage tissue is determined by its hierarchical structure along with collagen–proteoglycan biomechanical properties derived from the nanoscale level. Study of the atomic-scale structure and associated interactions in the native cartilage ECM guides in understanding the mechanism of degenerative cartilage diseases such as osteoarthritis, which starts with the fragmentation of proteoglycans followed by the disruption of the collagen network leading to cartilage loss.^{61,62} The polysaccharide unit (GAG) of proteoglycan plays a predominant role in cell signaling, development, angiogenesis, and cell proliferation.³⁵ Therefore, to probe the collagen–GAG correlation in the native cartilage ECM at the atomic level, we performed a 2D PMLG ^1H – ^{13}C HETCOR experiment employing a CP contact time of 200 μs . The 2D ^1H – ^{13}C HETCOR spectrum (Figure 3) shows the correlation between the resonances of GAGs and collagen residues. The chemical structure of the monomeric unit of GAGs (CS) is shown in Figure S3. Well-resolved resonances observed between 95 and 107 ppm arise from α and β GAG C1 carbons. The proton chemical shift for C1 of GAGs appears at 4.5–5.5 ppm, and for C5, it lies between 3.4 and 4.0 ppm as per the literature.^{58,63} GAG carbons are correlated with collagen protein residues through ^1H – ^{13}C dipolar coupling networks, which are in spatial proximity. The ^{13}C and ^1H slices of the cross-peak of interest from the 2D ^1H – ^{13}C HETCOR spectrum of cartilage are given in Figure S5A,B. GAG C1 (103 ppm) resonance shows a correlation with protons of Hyp C γ (71 ppm), Arg C α (54.5 ppm), Ala C α (49.2), and Hyp C β (38.5 ppm). A correlation between GAG C1 (96.3 ppm) and Gly C α (43 ppm) is observed. Similarly, GAG C1 resonances at 102.5 and 100.7 ppm show interactions with Ala C α (49.2 ppm), Lys C β (35.8 ppm), Arg C β (29.6 ppm), Lys C α (56.5 ppm), Asp C α

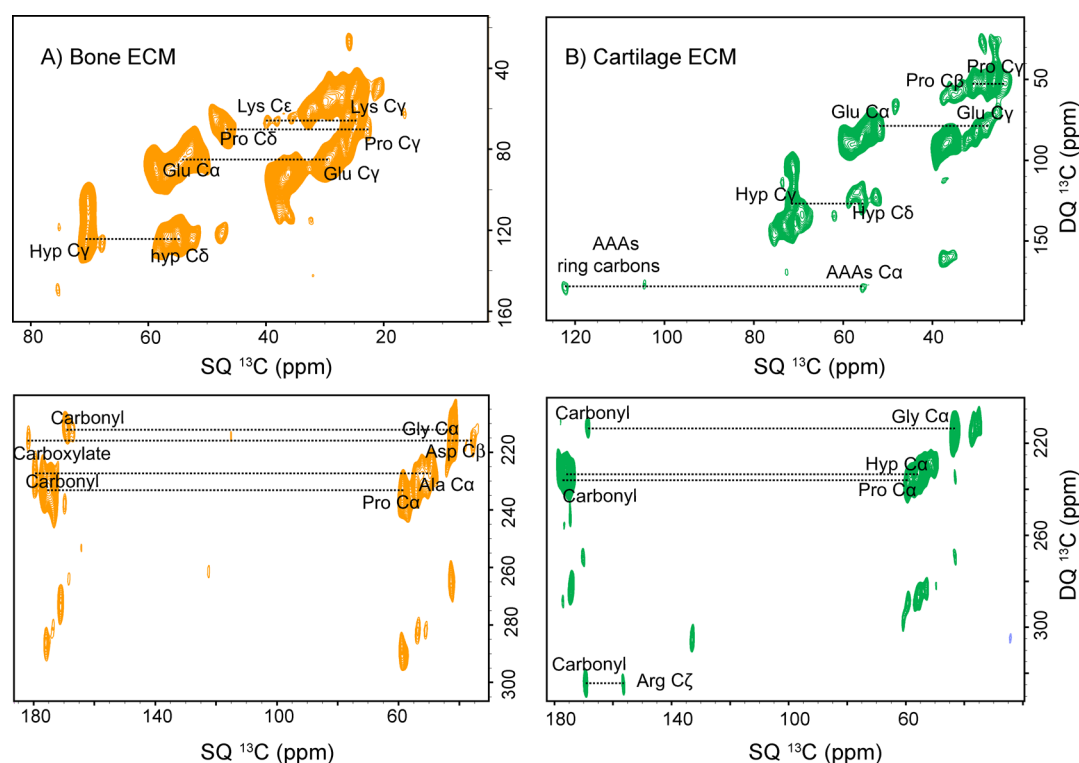


Figure 4. Natural-abundance 2D ^{13}C DQ– ^{13}C SQ spectra of (A) the bone ECM and (B) the cartilage ECM show short-range (one bond) and long-range (more than one bond) correlations among ^{13}C resonances of collagen protein.

(50.8 ppm), and Lys C ϵ (40.2 ppm) through ^1H – ^{13}C dipolar coupling networks, as represented in Figure 3. Besides this, the resonance at 116 ppm arising from protons of Trp C ζ 1/Tyr C ϵ 1 shows a correlation with GAG C5 (76.5 ppm). In a broader picture, GAG ring carbon resonances show molecular interactions with Hyp, Arg, Lys, Asp, and Gly, along with Trp/Tyr ring carbons. The negatively charged GAG unit forms charge-pair salt-bridge-type interaction with positively charged residues Arg/Lys of collagen protein,⁶⁴ while Hyp and Asp may be involved in hydrogen bonding with GAGs. Interaction of GAGs with aromatic residues suggests the existence of CH– π type interactions. The position and interactions between proteoglycan–GAGs and collagen fibrils are not fixed; they can conceivably break and reform reversibly.^{65,66} This unique property provides flexibility and cushioning to the cartilage tissue against applied mechanical stress. Apart from GAG–collagen interactions, we observed many non-specific (hydrogen bonding) and specific (hydrophobic and charged) interactions inside the collagen supra-assembly, as shown in Figure 3.

Further, to map the structural integrity of collagen protein inside the bone and cartilage ECMs through the ^{13}C – ^{13}C homonuclear dipolar coupling network, we performed the SPC5 experiment to obtain ^{13}C DQ– ^{13}C SQ correlation spectra by spinning samples at 8 kHz MAS rate [$\nu_{\text{H}}(^{13}\text{C}) = 40$ kHz] while employing a contact time of 1000 μs .^{67,68} Figure 4A, B shows the ^{13}C DQ– ^{13}C SQ spectra of bone and cartilage ECMs in natural isotopic abundance. In the ^{13}C DQ–SQ spectra of both ECMs, short- (one bond) and long-range correlations (more than one bond) are observed. The ^{13}C DQ– ^{13}C SQ spectrum indicates the ^{13}C – ^{13}C correlation arising from collagen protein resonances. A ^{13}C DQ– ^{13}C SQ correlation between aromatic AA ring carbons–aromatic AA C α and Arg C ζ –carbonyl carbon along with correlation

among the aliphatic residues of collagen protein in the ECM of cartilage indicate that the ^{13}C – ^{13}C dipolar coupling networks in both the ECMs are different from each other. The ^{13}C DQ– ^{13}C SQ experiments are useful in probing the structural difference in the collagen assembly because it enables mapping of the ^{13}C polarization transfer through the space inside the ECMs of the bone and cartilage in their native states.

3.3. Probing the Backbone and Side-Chain Interactions inside the Native Collagen Assembly. Due to the very low occurrence (0.37%) and low gyromagnetic ratio (-2.7126×10^7 rad T^{-1} s^{-1}) of ^{15}N nuclei, acquiring ^{15}N spectra of collagen protein in natural isotopic abundance is beyond the ssNMR detection limits.⁶⁹ Therefore, to probe the backbone structure along with side chains of other basic residues (Arg and Lys) of native collagen protein in bone and cartilage matrices without ^{15}N labeling, we have utilized the DNP-based ^{15}N ssNMR experiments. The 1D ^1H – ^{15}N CPMAS spectra of bone and cartilage matrices are shown in Figure 5A,C. In the 1D ^1H – ^{15}N CPMAS spectrum of the bone (Figure 5A), we have assigned the resonances exclusively from Gly N (109.2 ppm), Hyp/Pro N (129.9 ppm), Arg N ϵ (82.5 ppm), Arg N η (71.0 ppm), Lys N ζ (38 and 31.7 ppm), and Trp N ϵ (138 ppm). Similarly, the resonances exclusively from Gly N (109.2 ppm), Hyp/Pro N (129.8 ppm), Arg N ϵ (82.3 ppm), Arg N η (71.3 ppm), Lys N ζ (37.1 and 29.1 ppm), and Trp N ϵ (138 ppm) are assigned for the 1D ^1H – ^{15}N CPMAS spectrum of the cartilage (Figure 5C).^{70,71} In both matrices, ^{15}N resonances from collagen protein are observed at nearly the same chemical shift except for Lys N ζ (38 and 31.7 ppm), evidencing a different chemical environment around the Lys residue. Remarkable sensitivity enhancement in natural-abundance 1D ^1H – ^{15}N CPMAS spectra directs us to record further the 2D ^1H – ^{15}N HETCOR spectra of both samples. The 2D PMLG ^1H – ^{15}N HETCOR spectra reveal a different

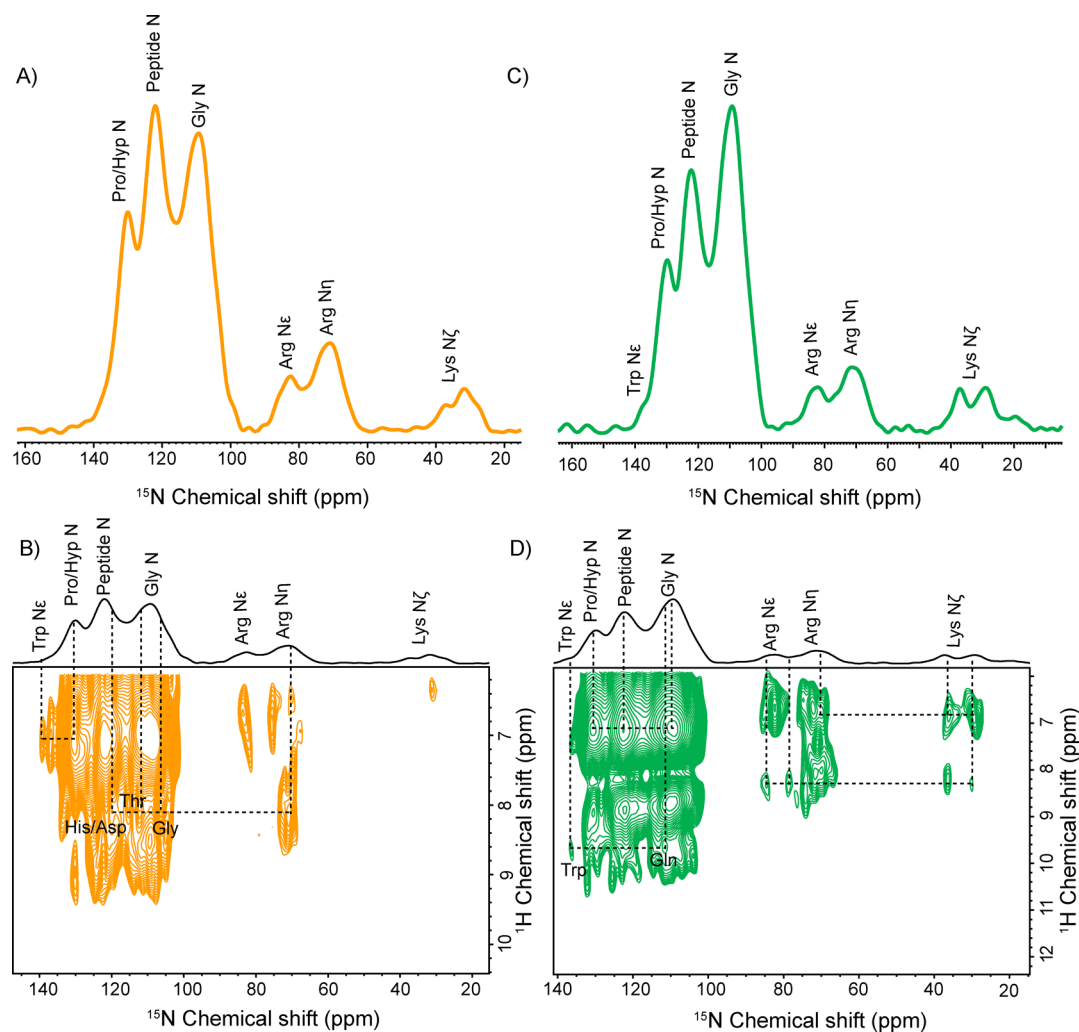


Figure 5. Natural-abundance (A) DNP-enhanced 1D ^1H - ^{15}N CPMAS of the bone ECM with assigned resonances. (B) 2D PMLG ^1H - ^{15}N HETCOR spectrum of the bone ECM with molecular interaction between ^{15}N resonances of various residues of collagen protein. (C) DNP-enhanced 1D ^1H - ^{15}N CPMAS of the cartilage ECM with assigned resonances. (D) 2D PMLG ^1H - ^{15}N HETCOR spectrum of the cartilage ECM with molecular interaction between ^{15}N resonances of various residues of collagen protein.

molecular arrangement of the backbone and side-chain residues in the collagen assembly inside bone and cartilage matrices (Figure 5B,D). The ^{15}N slices of the cross-peak of interest from the 2D ^1H - ^{15}N HETCOR spectrum of the cartilage are given in Figure S6. In Figure 5B, the molecular interactions between protons of Arg N ϵ -His N/Asp N (119.9 ppm), Arg N ϵ -Thr N, and Arg N ϵ -Gly N are observed through a ^1H - ^{15}N dipolar coupling network in the spatial proximity of the collagen assembly. Arg side-chains form cation- π interactions with aromatic AAs and cation-pair interactions with the acidic AAs in collagen protein. A correlation between protons of Pro/Hyp N and Trp N ϵ is observed. It has been reported earlier that Pro/Hyp shows CH- π interactions with aromatic AAs. These hydrophobic interactions, including cation- π , CH- π , and cation-pair interactions, add specificity and extra stability to the higher-order structure of collagen protein. The 2D ^1H - ^{15}N HETCOR spectrum of the cartilage ECM shows different molecular interactions from the bone ECM. A correlation is observed between Pro/Hyp N-Gly N, showing that these residues are involved in interstrand hydrogen bonding in collagen protein. Molecular interactions between protons of Trp N ϵ -Gln N, Arg N ϵ -Lys N ζ , and Arg N η -Lys N ζ are observed. The intra-molecular Arg-Lys

residues are involved in the advanced glycation end product (AGE) cross-linking sites in collagen protein.⁷² The properties of collagenous tissues are adversely affected by the formation of AGE. Besides this, they are even linked to the presence of several age-related disorders.⁷² Thus, probing molecular interaction through the 2D ^1H - ^{15}N HETCOR experiment may help elucidate the structural disorders associated with disease conditions in the bone and cartilage.

The huge gain in sensitivity makes DNP-MAS ssNMR methods preferable in elucidating the structure details of such complex heterogeneous systems. In the process of acquiring MAS-DNP ssNMR spectra, some challenges were faced. In sample preparation, the sizes of the powder particles, particularly in the case of the cartilage samples, are relatively large such that the size of a single particle can reach tens to hundreds of micrometers in diameter. Thus, rather than obtaining a spectrum evenly for the entire sample particle, the surface of the particle that is close to the DNP juice would be oversampled. This limitation can be reduced by making the sample into a fine granular powder or by penetrating the radicals in the DNP juice deeper into the core of the sample particle if the matrix of the sample possesses porous pores. In addition, a line broadening effect is also seen in cartilage

spectra, which is associated with the DNP sampling condition for making a glassy state, which causes the disorderliness of the molecular association that makes an asymmetrically broadened lineshape (the Czjzek lineshape).

4. CONCLUSIONS

Natural-abundance ssNMR experiments are challenging for elucidating the structural details of the complex heterogeneous biomaterials such as the bone and cartilage, but the impressive gains in sensitivity realized with MAS-DNP facilitates us to perform the 2D ^1H - ^{15}N , ^1H - ^{13}C HETCOR, and ^{13}C DQ- ^{13}C SQ experiments. With the help of these experiments, we were able to probe collagen-citrate (the bone ECM) and collagen-GAGs (the cartilage ECM), along with the other molecular interactions in the collagen protein assembly in both the ECM. From the 2D ^1H - ^{13}C HETCOR spectra, it was depicted that citrate shows molecular interactions with Arg, Glu Ala, and aromatic AA residues of collagen protein inside the bone matrix. These findings confirmed that citrate is an integral component of the apatite-collagen nanocomposite in the bone matrix. Similarly, the direct interactions of GAG resonances with Hyp, Arg, Lys, Asp, and Gly, along with Trp/Tyr resonances of collagen protein inside the cartilage ECM, were observed in the 2D ^1H - ^{13}C HETCOR spectrum, indicating that GAG molecules involved in ionic and non-ionic interactions such as hydrogen bonds and hydrophobic interactions with AA residues of collagen protein, responsible for the stability of the cartilage ECM and their physicochemical properties. We differentiated the structural assembly of collagen by mapping the ^{13}C - ^{13}C dipolar coupling network in both the ECMs. Additionally, utilizing the 2D ^1H - ^{15}N HETCOR experiments in natural abundance, which were not possible earlier without DNP, gave insights into the backbone and side-chain structural map of the collagen matrix inside the bone and cartilage. The structural studies, along with molecular interaction in bone and cartilage ECMs, would be helpful in comprehending the structural-functional mechanism and their biomechanical properties, thus providing guidance in the development of prevention and care therapy for the diseases which are associated with bone and cartilage disorders.

Overall, the impressive gain in sensitivity encourages the possibility of performing DNP-enhanced ^{13}C - ^{13}C as well as ^{13}C - ^{15}N correlation, REDOR/RR-type experiments, and various other 3D experiments to elucidate the 3D structural details in the absolute native environment of bones and cartilage at the natural isotopic abundance.

■ ASSOCIATED CONTENT

Supporting Information

The Supporting Information is available free of charge at <https://pubs.acs.org/doi/10.1021/acs.jpbc.1c01431>.

1D ^1H - ^{13}C CPMAS spectra of native collagen inside the bone matrix, with microwave ON and microwave OFF using the AMUPOL biradical; 1D ^1H - ^{13}C CPMAS spectra, 1D ^1H - ^{15}N CPMAS spectra, and 1D ^1H spectra of the bone matrix, with microwave ON and microwave OFF using the AsympolPOK biradical; chemical structure of citrate (the bone ECM) and the monomer unit of CS of GAGs (the cartilage ECM); ^{13}C slices and ^1H slices taken through cross-peaks of interest from the 2D ^1H - ^{13}C HETCOR spectrum of the bone

powder; ^{13}C slices taken through cross-peaks of interest from the 2D ^1H - ^{13}C HETCOR spectrum of the cartilage; ^1H slices taken through cross-peaks of interest from the 2D ^1H - ^{13}C HETCOR spectrum of the cartilage; ^{15}N slices taken through cross-peaks of interest (Figure 5) from the 2D ^1H - ^{15}N HETCOR spectrum of the bone and cartilage; full cross-section in the ^{13}C dimension of 2D PMLG ^1H - ^{13}C HETCOR spectra of the bone ECM and cartilage ECM; and asymmetrically broadened Czjzek lineshape in the projection of the ^1H dimension in the ^1H - ^{13}C HETCOR spectrum of the cartilage (PDF)

■ AUTHOR INFORMATION

Corresponding Author

Neeraj Sinha – Centre of Biomedical Research, Lucknow 226014, India; orcid.org/0000-0003-3235-6127;
Email: neerajcbmr@gmail.com, neeraj.sinha@cbmr.res.in

Authors

Nidhi Tiwari – Centre of Biomedical Research, Lucknow 226014, India; Department of Chemistry, Institute of Sciences, Banaras Hindu University, Varanasi 221005, India
Sungsool Wi – National High Magnetic Field Laboratory, Tallahassee, Florida 32304, United States
Frederic Mentink-Vigier – National High Magnetic Field Laboratory, Tallahassee, Florida 32304, United States;
orcid.org/0000-0002-3570-9787

Complete contact information is available at:
<https://pubs.acs.org/doi/10.1021/acs.jpbc.1c01431>

Author Contributions

N.T. and N.S. conceived and designed the analysis. S.W. and F.M.-V. collected the data. N.T. and N.S. analyzed and interpreted the data. N.T. and N.S. drafted the article. S.W. and F.M.-V. critically revised the article. All the authors have accepted the responsibility for the entire content of the submitted manuscript and approved submission.

Notes

The authors declare no competing financial interest.

■ ACKNOWLEDGMENTS

The authors gratefully acknowledge the SERB (EMR/2015/001758) and the Council of Scientific and Industrial Research (CSIR), India, for financial support. The authors are also thankful to the National High Magnetic Field Laboratory, Tallahassee, Florida, which is supported by the NIH P41 GM122698, NIH S10 OD018519, and the National Science Foundation Cooperative Agreement no. DMR-1644779. We also acknowledge Prof. RamaNand Rai and Navneet Dwivedi for their valuable suggestions and help.

■ REFERENCES

- (1) Hall, B. K. *Bones and Cartilage: Developmental and Evolutionary Skeletal Biology*, 2nd ed.; Elsevier Inc., 2015.
- (2) McKee, T. J.; Perlman, G.; Morris, M.; Komarova, S. V. Extracellular Matrix Composition of Connective Tissues: A Systematic Review and Meta-Analysis. *Sci. Rep.* **2019**, *9*, 10542.
- (3) Shoulders, M. D.; Raines, R. T. Collagen Structure and Stability. *Annu. Rev. Biochem.* **2009**, *78*, 929–958.
- (4) Gelse, K.; Pöschl, E.; Aigner, T. Collagens - Structure, Function, and Biosynthesis. *Adv. Drug Deliv. Rev.* **2003**, *55*, 1531–1546.

- (5) Bella, J.; Eaton, M.; Brodsky, B.; Berman, H. Crystal and Molecular Structure of a Collagen-like Peptide at 1.9 Å Resolution. *Science* **1994**, *266*, 75–81.
- (6) Aliev, A. E.; Courtier-Murias, D. Water Scaffolding in Collagen: Implications on Protein Dynamics as Revealed by Solid-State NMR. *Biopolymers* **2014**, *101*, 246–256.
- (7) Fu, I.; Case, D. A.; Baum, J. Dynamic Water-Mediated Hydrogen Bonding in a Collagen Model Peptide. *Biochemistry* **2015**, *54*, 6029–6037.
- (8) Rai, R. K.; Singh, C.; Sinha, N. Predominant Role of Water in Native Collagen Assembly inside the Bone Matrix. *J. Phys. Chem. B* **2015**, *119*, 201–211.
- (9) Rich, A.; Crick, F. H. C. The Molecular Structure of Collagen. *J. Mol. Biol.* **1961**, *3*, 483.
- (10) Jenkins, C. L.; Raines, R. T. Insights on the Conformational Stability of Collagen. *Nat. Prod. Rep.* **2002**, *19*, 49–59.
- (11) Singh, C.; Rai, R. K.; Aussenac, F.; Sinha, N. Direct Evidence of Imino Acid-Aromatic Interactions in Native Collagen Protein by DNP-Enhanced Solid-State NMR Spectroscopy. *J. Phys. Chem. Lett.* **2014**, *5*, 4044–4048.
- (12) Chen, C.-C.; Hsu, W.; Hwang, K.-C.; Hwu, J. R.; Lin, C.-C.; Horng, J.-C. Contributions of Cation- π Interactions to the Collagen Triple Helix Stability. *Arch. Biochem. Biophys.* **2011**, *508*, 46–53.
- (13) Kar, K.; Ibrar, S.; Nanda, V.; Getz, T. M.; Kunapuli, S. P.; Brodsky, B. Aromatic Interactions Promote Self-Association of Collagen Triple-Helical Peptides to Higher-Order Structures. *Biochemistry* **2009**, *48*, 7959–7968.
- (14) Bella, J.; Berman, H. M. Crystallographic Evidence for Ca–H...O=C Hydrogen Bonds in a Collagen Triple Helix. *J. Mol. Biol.* **1996**, *264*, 734–742.
- (15) Fallas, J. A.; Dong, J.; Tao, Y. J.; Hartgerink, J. D. Structural Insights into Charge Pair Interactions in Triple Helical Collagen-like Proteins. *J. Biol. Chem.* **2012**, *287*, 8039–8047.
- (16) Scott, J. E. Proteoglycan-Fibrillar Collagen Interactions. *Biochem. J.* **1988**, *252*, 313–323.
- (17) Irving, J. T. Calcification of the Organic Matrix of Enamel. *Arch. Oral Biol.* **1963**, *8*, 773.
- (18) Landis, W. J.; Song, M. J.; Leith, A.; McEwen, L.; McEwen, B. F. Mineral and Organic Matrix Interaction in Normally Calcifying Tendon Visualized in Three Dimensions by High-Voltage Electron Microscopic Tomography and Graphic Image Reconstruction. *J. Struct. Biol.* **1993**, *110*, 39–54.
- (19) Bonucci, E. Fine Structure of Early Cartilage Calcification. *J. Ultrastruct. Res.* **1967**, *20*, 33–50.
- (20) Tiwari, N.; Rai, R.; Sinha, N. Water-Lipid Interactions in Native Bone by High-Resolution Solid-State NMR Spectroscopy. *Solid State Nucl. Magn. Reson.* **2020**, *107*, 101666.
- (21) Reid, D. G.; Duer, M. J.; Jackson, G. E.; Murray, R. C.; Rodgers, A. L.; Shanahan, C. M. Citrate Occurs Widely in Healthy and Pathological Apatitic Biomineral: Mineralized Articular Cartilage, and Intimal Atherosclerotic Plaque and Apatitic Kidney Stones. *Calcif. Tissue Int.* **2013**, *93*, 253–260.
- (22) Dickens, F. The Citric Acid Content of Animal Tissues, with Reference to Its Occurrence in Bone and Tumour. *Biochem. J.* **1941**, *35*, 1011–1023.
- (23) Shao, C.; Zhao, R.; Jiang, S.; Yao, S.; Wu, Z.; Jin, B.; Yang, Y.; Pan, H.; Tang, R. Citrate Improves Collagen Mineralization via Interface Wetting: A Physicochemical Understanding of Biomineralization Control. *Adv. Mater.* **2018**, *30*, 1704876.
- (24) Davies, E.; Müller, K. H.; Wong, W. C.; Pickard, C. J.; Reid, D. G.; Skepper, J. N.; Duer, M. J. Citrate Bridges between Mineral Platelets in Bone. *Proc. Natl. Acad. Sci. U.S.A.* **2014**, *111*, No. E1354.
- (25) Norman, A. W.; Deluca, H. F. Vitamin D and the Incorporation of [1-¹⁴C]Acetate into the Organic Acids of. *Biochem. J.* **1964**, *91*, 124.
- (26) Hu, Y.-Y.; Liu, X. P.; Ma, X.; Rawal, A.; Prozorov, T.; Akinc, M.; Mallapragada, S. K.; Schmidt-Rohr, K. Biomimetic Self-Assembling Copolymer-Hydroxyapatite Nanocomposites with the Nanocrystal Size Controlled by Citrate. *Chem. Mater.* **2011**, *23*, 2481–2490.
- (27) Hu, Y. Y.; Rawal, A.; Schmidt-Rohr, K. Strongly Bound Citrate Stabilizes the Apatite Nanocrystals in Bone. *Proc. Natl. Acad. Sci. U.S.A.* **2010**, *107*, 22425–22429.
- (28) Costello, L. C.; Chellaiiah, M.; Zou, J.; Franklin, R. B.; Reynolds, M. A. The Status of Citrate in the Hydroxyapatite/Collagen Complex of Bone; and Its Role in Bone Formation. *J. Regen. Med. Tissue Eng.* **2014**, *3*, 4.
- (29) Sophia Fox, A. J.; Bedi, A.; Rodeo, S. A. The Basic Science of Articular Cartilage: Structure, Composition, and Function. *Sport Health* **2009**, *1*, 461–468.
- (30) Ricard-Blum, S.; Ruggiero, F. The Collagen Superfamily: From the Extracellular Matrix to the Cell Membrane. *Pathol. Biol.* **2005**, *53*, 430–442.
- (31) Huster, D. Chapter 4 Solid-State NMR Studies of Collagen Structure and Dynamics in Isolated Fibrils and in Biological Tissues. *Annu. Rep. NMR Spectrosc.* **2008**, *64*, 127–159.
- (32) Poole, A. R. Proteoglycans in Health and Disease: Structures and Functions. *Biochem. J.* **1986**, *236*, 1–14.
- (33) Heinegård, D. Proteoglycans and More - From Molecules to Biology. *Int. J. Exp. Pathol.* **2009**, *90*, 575–586.
- (34) Yoon, J. H.; Halper, J. Tendon Proteoglycans: Biochemistry and Function. *J. Musculoskelet. Neuronal Interact.* **2005**, *5*, 22–34.
- (35) Gandhi, N. S.; Mancera, R. L. The Structure of Glycosaminoglycans and Their Interactions with Proteins. *Chem. Biol. Drug Des.* **2008**, *72*, 455–482.
- (36) Rojas, F. P.; Batista, M. A.; Lindburg, C. A.; Dean, D.; Grodzinsky, A. J.; Ortiz, C.; Han, L. Molecular Adhesion between Cartilage Extracellular Matrix Macromolecules. *Biomacromolecules* **2014**, *15*, 772–780.
- (37) Mroue, K. H.; Viswan, A.; Sinha, N.; Ramamoorthy, A. *Solid-State NMR Spectroscopy: The Magic Wand to View Bone at Nanoscopic Resolution*, 1st ed.; Elsevier Ltd., 2017; Vol. 92.
- (38) Xu, J.; Zhu, P.; Morris, M. D.; Ramamoorthy, A. Solid-State NMR Spectroscopy Provides Atomic-Level Insights into the Dehydration of Cartilage. *J. Phys. Chem. B* **2011**, *115*, 9948–9954.
- (39) Mroue, K. H.; Nishiyama, Y.; Kumar Pandey, M.; Gong, B.; McNerny, E.; Kohn, D. H.; Morris, M. D.; Ramamoorthy, A. Proton-Detected Solid-State NMR Spectroscopy of Bone with Ultrafast Magic Angle Spinning. *Sci. Rep.* **2015**, *5*, 11991.
- (40) Singh, C.; Rai, R. K.; Kayastha, A. M.; Sinha, N. Ultra Fast Magic Angle Spinning Solid - State NMR Spectroscopy of Intact Bone. *Magn. Reson. Chem.* **2016**, *54*, 132–135.
- (41) Hassan, A.; Quinn, C. M.; Struppe, J.; Sergeev, I. V.; Zhang, C.; Guo, C.; Runge, B.; Theint, T.; Dao, H. H.; Jaroniec, C. P.; et al. Sensitivity Boosts by the CPMAS CryoProbe for Challenging Biological Assemblies. *J. Magn. Reson.* **2020**, *311*, 106680.
- (42) Tiwari, N.; Wegner, S.; Hassan, A.; Dwivedi, N.; Rai, R.; Sinha, N. Probing Short and Long-Range Interactions in Native Collagen inside the Bone Matrix by BioSolids CryoProbe. *Magn. Reson. Chem.* **2021**, *59*, 99.
- (43) Hall, D. A.; Maus, D. C.; Gerfen, G. J.; Inati, S. J.; Becerra, L. R.; Dahlquist, F. W.; Griffin, R. G. Polarization-Enhanced NMR Spectroscopy of Biomolecules in Frozen Solution. *Science* **1997**, *276*, 930–932.
- (44) Hediger, S.; Lee, D.; Mentink-Vigier, F.; De Paëpe, G. MAS-DNP Enhancements: Hyperpolarization, Depolarization, and Absolute Sensitivity. *eMagRes* **2018**, *7*, 105–116.
- (45) Kundu, K.; Mentink-Vigier, F.; Feintuch, A.; Vega, S. DNP Mechanisms. *eMagRes* **2019**, *8*, 295–338.
- (46) Lee, D.; Hediger, S.; De Paëpe, G. Is Solid-State NMR Enhanced by Dynamic Nuclear Polarization?. *Solid State Nuclear Magnetic Resonance*; Elsevier, 2015; Vol. 66–67, pp 6–20.
- (47) Yamamoto, K.; Caporini, M. A.; Im, S.-C.; Waskell, L.; Ramamoorthy, A. Cellular Solid-State NMR Investigation of a Membrane Protein Using Dynamic Nuclear Polarization. *Biochim. Biophys. Acta, Biomembr.* **2015**, *1848*, 342–349.

- (48) Kang, X.; Kirui, A.; Dickwella Widanage, M. C.; Mentink-Vigier, F.; Cosgrove, D. J.; Wang, T. Lignin-Polysaccharide Interactions in Plant Secondary Cell Walls Revealed by Solid-State NMR. *Nat. Commun.* **2019**, *10*, 347.
- (49) Rossini, A. J.; Zagdoun, A.; Hegner, F.; Schwarzwälder, M.; Gajan, D.; Copéret, C.; Lesage, A.; Emsley, L. Dynamic Nuclear Polarization NMR Spectroscopy of Microcrystalline Solids. *J. Am. Chem. Soc.* **2012**, *134*, 16899–16908.
- (50) Takahashi, H.; Hediger, S.; De Paëpe, G. Matrix-Free Dynamic Nuclear Polarization Enables Solid-State NMR ^{13}C - ^{13}C Correlation Spectroscopy of Proteins at Natural Isotopic Abundance. *Chem. Commun.* **2013**, *49*, 9479–9481.
- (51) Chow, W. Y.; Norman, B. P.; Roberts, N. B.; Ranganath, L. R.; Teutloff, C.; Bittl, R.; Duer, M. J.; Gallagher, J. A.; Oschkinat, H. Pigmentation Chemistry and Radical-Based Collagen Degradation in Alkaptonuria and Osteoarthritic Cartilage. *Angew. Chem., Int. Ed.* **2020**, *59*, 11937.
- (52) Sauvée, C.; Rosay, M.; Casano, G.; Aussenac, F.; Weber, R. T.; Ouari, O.; Tordo, P. Highly Efficient, Water-Soluble Polarizing Agents for Dynamic Nuclear Polarization at High Frequency. *Angew. Chem., Int. Ed.* **2013**, *52*, 10858–10861.
- (53) Dubroca, T.; Smith, A. N.; Pike, K. J.; Froud, S.; Wylde, R.; Trociewitz, B.; McKay, J.; Mentink-Vigier, F.; van Tol, J.; Wi, S.; et al. A Quasi-Optical and Corrugated Waveguide Microwave Transmission System for Simultaneous Dynamic Nuclear Polarization NMR on Two Separate 14.1 T Spectrometers. *J. Magn. Reson.* **2018**, *289*, 35–44.
- (54) Rienstra, C. M.; Jaroniec, C. P.; Hohwy, M.; Rienstra, C. M.; Jaroniec, C. P.; Griffin, R. G. Fivefold Symmetric Homonuclear Dipolar Recoupling in Rotating Solids: Application To Double Quantum Spectroscopy. *Artic. J. Chem. Phys.* **1999**, *110*, 7983–7992.
- (55) Vinogradov, E.; Madhu, P. K.; Vega, S. Phase Modulated Lee-Goldburg Magic Angle Spinning Proton Nuclear Magnetic Resonance Experiments in the Solid State: A Bimodal Floquet Theoretical Treatment. *J. Chem. Phys.* **2001**, *115*, 8983–9000.
- (56) Fung, B. M.; Khitrin, A. K.; Ermolaev, K. An Improved Broadband Decoupling Sequence for Liquid Crystals and Solids. *J. Magn. Reson.* **2000**, *142*, 97–101.
- (57) Rai, R. K.; Sinha, N. Dehydration-Induced Structural Changes in the Collagen-Hydroxyapatite Interface in Bone by High-Resolution Solid-State NMR Spectroscopy. *J. Phys. Chem. C* **2011**, *115*, 14219–14227.
- (58) Pomin, V. H. NMR Chemical Shifts in Structural Biology of Glycosaminoglycans. *Anal. Chem.* **2014**, *86*, 65–94.
- (59) Ni, Q. Z.; Markhasin, E.; Can, T. V.; Corzilius, B.; Tan, K. O.; Barnes, A. B.; Daviso, E.; Su, Y.; Herzfeld, J.; Griffin, R. G. Peptide and Protein Dynamics and Low-Temperature/DNP Magic Angle Spinning NMR. *J. Phys. Chem. B* **2017**, *121*, 4997–5006.
- (60) Takahashi, H.; Fernández-de-Alba, C.; Lee, D.; Maurel, V.; Gambarelli, S.; Bardet, M.; Hediger, S.; Barra, A.-L.; De Paëpe, G. Optimization of an Absolute Sensitivity in a Glassy Matrix during DNP-Enhanced Multidimensional Solid-State NMR Experiments. *J. Magn. Reson.* **2014**, *239*, 91–99.
- (61) Hardingham, T. Chondroitin Sulfate and Joint Disease. *Osteoarthr. Cartil.* **1998**, *6*, 3–5.
- (62) Vinatier, C.; Guicheux, J. Cartilage Tissue Engineering: From Biomaterials and Stem Cells to Osteoarthritis Treatments. *Annals of Physical and Rehabilitation Medicine*; Elsevier Masson SAS, 2016; Vol. 59, pp 139–144.
- (63) Toida, T.; Toyoda, H. High-Resolution Proton on Chondroitin Sulfates Nuclear Magnetic Resonance Studies. *Anal. Sci.* **1993**, *9*, 53.
- (64) Joseph, P. R. B.; Sawant, K. V.; Iwahara, J.; Garofalo, R. P.; Desai, U. R.; Rajarathnam, K. Lysines and Arginines Play Non-Redundant Roles in Mediating Chemokine-Glycosaminoglycan Interactions. *Sci. Rep.* **2018**, *8*, 12289.
- (65) Scott, J. E. Elasticity in Extracellular Matrix “shape Modules” of Tendon, Cartilage, Etc. A Sliding Proteoglycan-Filament Model. *J. Physiol.* **2003**, *553*, 335–343.
- (66) Lewis, P. N.; Pinali, C.; Young, R. D.; Meek, K. M.; Quantock, A. J.; Knupp, C. Structural Interactions between Collagen and Proteoglycans Are Elucidated by Three-Dimensional Electron Tomography of Bovine Cornea. *Structure* **2010**, *18*, 239–245.
- (67) Su, Y.; Hong, M. Conformational Disorder of Membrane Peptides Investigated from Solid-State NMR Line Widths and Line Shapes. *J. Phys. Chem. B* **2011**, *115*, 10758–10767.
- (68) Hohwy, M.; Rienstra, C. M.; Jaroniec, C. P.; Griffin, R. G. Fivefold Symmetric Homonuclear Dipolar Recoupling in Rotating Solids: Application to Double Quantum Spectroscopy. *J. Chem. Phys.* **1999**, *110*, 7983–7992.
- (69) Gutmann, T.; Liu, J.; Rothermel, N.; Xu, Y.; Jaumann, E.; Werner, M.; Breitzke, H.; Sigurdsson, S. T.; Buntkowsky, G. Natural Abundance ^{15}N NMR by Dynamic Nuclear Polarization: Fast Analysis of Binding Sites of a Novel Amine-Carboxyl-Linked Immobilized Dirhodium Catalyst. *Chem.—Eur. J.* **2015**, *21*, 3798–3805.
- (70) Goldberga, I.; Li, R.; Chow, W. Y.; Reid, D. G.; Bashtanova, U.; Rajan, R.; Puzzkarska, A.; Oschkinat, H.; Duer, M. J. Detection of Nucleic Acids and Other Low Abundance Components in Native Bone and Osteosarcoma Extracellular Matrix by Isotope Enrichment and DNP-Enhanced NMR. *RSC Adv.* **2019**, *9*, 26686–26690.
- (71) Singh, C.; Sinha, N. Mechanistic Insights into the Role of Water in Backbone Dynamics of Native Collagen Protein by Natural Abundance ^{15}N NMR Spectroscopy. *J. Phys. Chem. C* **2016**, *120*, 9393–9398.
- (72) Collier, T. A.; Nash, A.; Birch, H. L.; de Leeuw, N. H. Intra-Molecular Lysine-Arginine Derived Advanced Glycation End-Product Cross-Linking in Type I Collagen: A Molecular Dynamics Simulation Study. *Biophys. Chem.* **2016**, *218*, 42–46.